Linear Analysis of the Currents in a Pipe

U. Brosa

Fachbereich Physik der Philipps-Universität, Marburg

Z. Naturforsch. **41 a**, 1141 – 1153 (1986); received June 5, 1986

A simple procedure to find solutions of the hydrodynamic Stokes equations is given. The procedure is used to determine the linear modes of a newtonian fluid in a pipe of circular cross section. Compressibility, shear and bulk viscosity are included, and no restrictions on the symmetry of the modes are made. Furthermore an infinite set of exact solutions of the Navier-Stokes equations is presented.

1. Introduction

Despite of its apparent simplicity and ubiquitous presence the familar pipe filled with water remains one of the most mysterious objects in physics. It is known experimentally that the laminar flow undergoes a transition to turbulence when it becomes too fast, usually at a Reynolds number of about 2000. But while theoretically for similar systems, viz. the Blasius boundary layer and the rectangular channel, an instability was found which can be interpreted as the entrance door to turbulence, a similar analysis for the pipe failed completely [1, pp. 216 – 221]. Moreover, careful experiments have shown that the Reynolds number 2000 has to be replaced by a much larger value when very straight and smooth pipes are used, when the inlet of flow is favorably shaped, and when vibrations are kept away from the system [2, pp. 454 – 458], [3]. These theoretical and experimental results led to the belief that in a pipe turbulence can only be created by perturbations which are too large to permit linear analysis. Nonlinear analysis indeed shows amplification of certain perturbations. It is, however, not simple to correlate these findings with experiments, as is discussed e.g. by Sen et al. [4].

Surprisingly enough, some inspection of the literature reveals that even the linear modes of the Stokes problem do not seem to be elaborated in full. Either only axially symmetrical modes were considered, or bulk viscosity and compressibility neglected, or improper boundary conditions imposed [2, pp. 9 – 12, p. 94, pp. 441 – 443]. It is the purpose of the present paper to present the Stokes modes without any of these restrictions.

Lessen, Sadler and Liu [5] as well as Salwen and Grosch [6] approached a more difficult problem, viz. the linearisation of the Navier-Stokes equations in the vicinity of the Hagen-Poiseuille solution, whereas here the Navier-Stokes equations are linearized about the zero-velocity solution. The excuses for the present paper are, first, that the Stokes modes can be given in comparatively simple analytical terms, second, that these modes may serve as a basis for series expansions to solve higher order problems and, third, that the search for the Stokes modes yields an infinite set of exact solutions of the complete Navier-Stokes equations for incompressible flow.

The obtainment of the results on the Stokes modes in the pipe was facilitated by the discovery of a representation theorem which seems to be generally useful in connection with Stokes problems. This theorem is presented in the second section and derived in the appendix. The third section contains the determination of the Stokes modes in the circular pipe, the solution of the characteristic equation, and a discussion of the most striking physical properties of the various modes. In this context also the exact solutions are revealed. Finally the significance of the results for further research is pointed out.

2. A Representation Theorem for Compressible Stokes Flow

As the starting point we take the Navier-Stokes equations for a compressible newtonian fluid [7, pp.

Reprint requests to Dr. U. Brosa, Fachbereich Physik der Philipps-Universität, Renthof 6, 3550 Marburg.

0340-4811 / 86 / 0900-1141 $ 01.30/0. – Please order a reprint rather than making your own copy.

151–164]

$$\varrho(\boldsymbol{r},t)\, d_t \boldsymbol{u}(\boldsymbol{r},t) = -\nabla p(\boldsymbol{r},t) + (\tfrac{4}{3}\eta + \lambda)\,\nabla(\nabla \boldsymbol{u}(\boldsymbol{r},t)) - \eta\,\nabla x(\nabla x\, \boldsymbol{u}(\boldsymbol{r},t)), \tag{1}$$

$$\partial_t \varrho(\boldsymbol{r},t) = -\nabla(\varrho(\boldsymbol{r},t)\, \boldsymbol{u}(\boldsymbol{r},t)), \tag{2}$$

$$p(\boldsymbol{r},t) = f(\varrho(\boldsymbol{r},t)) \tag{3}$$

which are valid for either isothermal or isentropic motions, depending on the equation of state (3). These equations are linearized by taking the velocity field $\boldsymbol{u}(\boldsymbol{r},t)$ as small of first order and replacing the pressure $p(\boldsymbol{r},t)$ by $p_0 + p(\boldsymbol{r},t)$, the density $\varrho(\boldsymbol{r},t)$ by $\varrho_0 + \varrho(\boldsymbol{r},t)$, and shear and bulk viscosities η and λ by $\eta_0 + \eta(\boldsymbol{r},t)$ and $\lambda_0 + \lambda(\boldsymbol{r},t)$, respectively, where all replaced functions should be regarded as small of first order, and p_0, ϱ_0, η_0 and λ_0 denote constants. Linearization has the effect of simplifying the total time derivative d_t in (1)

$$d_t \boldsymbol{u}(\boldsymbol{r},t) = \partial_t \boldsymbol{u}(\boldsymbol{r},t) + (\boldsymbol{u}(\boldsymbol{r},t)\,\nabla)\,\boldsymbol{u}(\boldsymbol{r},t), \tag{4}$$

so that only the partial derivative ∂_t remains. The equation of state (3) becomes

$$p(\boldsymbol{r},t) = c_c^2\, \varrho(\boldsymbol{r},t), \tag{5}$$

where c_c is a further constant which has the dimensions of a velocity. Introducing the abbreviations

$$\mu_0 = (\tfrac{4}{3}\eta_0 + \lambda_0)/\varrho_0, \quad \nu_0 = \eta_0/\varrho_0 \tag{6}$$

and eliminating the density perturbation $\varrho(\boldsymbol{r},t)$ we arrive at

$$\partial_t \boldsymbol{u}(\boldsymbol{r},t) = -\nabla p(\boldsymbol{r},t)/\varrho_0 + \mu_0 \nabla(\nabla \boldsymbol{u}(\boldsymbol{r},t)) - \nu_0 \nabla x(\nabla x\, \boldsymbol{u}(\boldsymbol{r},t)), \tag{7}$$

$$\partial_t p(\boldsymbol{r},t) = -\varrho_0 c_c^2 \nabla \boldsymbol{u}(\boldsymbol{r},t). \tag{8}$$

These are the Stokes equations for compressible flow. The components of the velocity field $\boldsymbol{u}(\boldsymbol{r},t)$ and the pressure perturbation $p(\boldsymbol{r},t)$ are coupled by these equations in a way which is particularly unpleasant when curvilinear coordinates are used. Here a representation theorem is useful: Instead of the Stokes equations we obtain three decoupled scalar differential equations.

The Stokes equations (7) and (8) are solved by the representation formulae

$$\boldsymbol{u}(\boldsymbol{r},t) = \nabla x(\boldsymbol{v}\, a(\boldsymbol{r},t)) + \nabla x(\nabla x(\boldsymbol{v}\, b(\boldsymbol{r},t))) + \nabla c(\boldsymbol{r},t), \tag{9}$$

$$p(\boldsymbol{r},t) = p_0 - \varrho_0\, \partial_t c(\boldsymbol{r},t)) + \mu_0\, \varrho_0\, \nabla^2 c(\boldsymbol{r},t) \tag{10}$$

if the potentials obey the differential equations

$$\frac{1}{\nu_0}\,\partial_t a(\boldsymbol{r},t) = \nabla^2 a(\boldsymbol{r},t), \tag{11}$$

$$\frac{1}{\nu_0}\,\partial_t b(\boldsymbol{r},t) = \nabla^2 b(\boldsymbol{r},t), \tag{12}$$

$$\frac{1}{c_c^2}\,\partial_t^2 c(\boldsymbol{r},t) = \nabla^2 c(\boldsymbol{r},t) + \frac{\mu_0}{c_c^2}\nabla^2\,\partial_t c(\boldsymbol{r},t), \tag{13}$$

and the supporting vector field $\boldsymbol{v}$ takes the form

$$\boldsymbol{v} = \boldsymbol{v}_0 + v_1 \boldsymbol{r}, \tag{14}$$

where $\boldsymbol{v}_0$ and v_1 denote an arbitrary but constant vector and scalar, respectively. Equation (14) is the most general form of the supporting vector field if the potentials $a(\boldsymbol{r},t)$ and $b(\boldsymbol{r},t)$ are to be independent of it.

The proof of this theorem will be given in the appendix.

3. Currents in a Pipe

a) The Basic Formulae

The computation of the Stokes modes in a circular pipe is a simple application of the theorem of the preceeding section. Of course we take cylindrical coordinates (r, φ, z) and choose as supporting vector field $\boldsymbol{v} = \boldsymbol{e}_z$, i.e. the unit vector in z direction. Separation of the differential equations (11)–(13) gives the three potentials

$$\begin{aligned} \boldsymbol{v}\, a(\boldsymbol{r},t) &= \boldsymbol{e}_z\, a_0 J_m\left(\sqrt{\frac{\sigma}{\nu_0} - k^2}\; r\right) \cdot e^{im\varphi} e^{ikz} e^{-\sigma t}, \\ \boldsymbol{v}\, b(\boldsymbol{r},t) &= \boldsymbol{e}_z\, b_0 J_m\left(\sqrt{\frac{\sigma}{\nu_0} - k^2}\; r\right) \cdot e^{im\varphi} e^{ikz} e^{-\sigma t}, \\ c(\boldsymbol{r},t) &= c_0 J_m\left(-\sqrt{\frac{\sigma^2}{\mu_0\sigma - c_c^2} - k^2}\; r\right) \cdot e^{im\varphi} e^{ikz} e^{-\sigma t}. \end{aligned} \tag{15}$$

m, k and σ are the usual separation constants with m being an integer while k and σ are permitted to be complex. a_0, b_0 and c_0 are complex constants which will be determined, up to normalization, by the boundary conditions. But first we compute from

(15) and (10) the pressure

$$p(\boldsymbol{r}, t) = p_0 + \frac{\varrho_0 c_c^2 \sigma}{c_c^2 - \mu_0 \sigma} c_0 J_m\left(-\sqrt{\frac{\sigma^2}{\mu_0 \sigma - c_c^2} - k^2}\, r\right) e^{im\varphi} e^{ikz} e^{-\sigma t}. \tag{16}$$

The spatial differentiations in (10) can be avoided if the differential equation (13) is used. Next we obtain from (15) and (9) the velocity field

$$\begin{aligned}
\boldsymbol{u}(r, \varphi, z, t) = \Bigg\{ & \boldsymbol{e}_r \cdot \left(a_0 \left(\frac{i m}{r} J_m\left(\sqrt{\frac{\sigma}{\nu_0} - k^2}\, r\right)\right) + b_0 \left(i k \sqrt{\frac{\sigma}{\nu_0} - k^2}\, J'_m\left(\sqrt{\frac{\sigma}{\nu_0} - k^2}\, r\right)\right)\right. \\
& \left. + c_0 \left(-\sqrt{\frac{\sigma^2}{\mu_0 \sigma - c_c^2} - k^2}\, J'_m\left(-\sqrt{\frac{\sigma^2}{\mu_0 \sigma - c_c^2} - k^2}\, r\right)\right)\right) + \\
& \boldsymbol{e}_\varphi \cdot \left(a_0 \left(-\sqrt{\frac{\sigma}{\nu_0} - k^2}\, J'_m\left(\sqrt{\frac{\sigma}{\nu_0} - k^2}\, r\right)\right) + b_0 \left(-\frac{m k}{r} J_m\left(\sqrt{\frac{\sigma}{\nu_0} - k^2}\, r\right)\right)\right. \\
& \left. + c_0 \left(\frac{i m}{r} J_m\left(-\sqrt{\frac{\sigma^2}{\mu_0 \sigma - c_c^2} - k^2}\, r\right)\right)\right) + \\
& \boldsymbol{e}_z \cdot \left(b_0 \left(\left(\frac{\sigma}{\nu_0} - k^2 \right) J_m\left(\sqrt{\frac{\sigma}{\nu_0} - k^2}\, r\right)\right) + c_0 \left(i k J_m\left(-\sqrt{\frac{\sigma^2}{\mu_0 \sigma - c_c^2} - k^2}\, r\right)\right)\right) \Bigg\} \cdot e^{im\varphi} e^{ikz} e^{-\sigma t}.
\end{aligned} \tag{17}$$

Here it is advisable to utilize the differential equation (12) and the differential equation of Bessel functions to eliminate higher derivatives of the Bessel functions.

The liquid sticks to the wall $r = R$. This gives the boundary conditions $\boldsymbol{u}(r = R, \varphi, z, t) = \boldsymbol{0}$, altogether three scalar equations. With (17) we find a homogeneous linear system

$$\begin{aligned}
& \frac{a_0}{R} (i m J_m(\sqrt{\alpha^2 - \beta^2})) + \frac{b_0}{R^2} (i \beta \sqrt{\alpha^2 - \beta^2}\, J'_m(\sqrt{\alpha^2 - \beta^2})) \\
& \qquad + \frac{c_0}{R} \left(-\sqrt{\frac{\alpha^4}{\gamma \alpha^2 - \delta^2} - \beta^2}\, J'_m\left(-\sqrt{\frac{\alpha^4}{\gamma \alpha^2 - \delta^2} - \beta^2}\right)\right) = 0, \\
& \frac{a_0}{R} (-\sqrt{\alpha^2 - \beta^2}\, J'_m(\sqrt{\alpha^2 - \beta^2})) + \frac{b_0}{R^2} (-m \beta J_m(\sqrt{\alpha^2 - \beta^2})) \\
& \qquad + \frac{c_0}{R} \left(i m J_m\left(-\sqrt{\frac{\alpha^4}{\gamma \alpha^2 - \delta^2} - \beta^2}\right)\right) = 0, \\
& \frac{b_0}{R^2} ((\alpha^2 - \beta^2) J_m(\sqrt{\alpha^2 - \beta^2})) + \frac{c_0}{R} \left(i \beta J_m\left(-\sqrt{\frac{\alpha^4}{\gamma \alpha^2 - \delta^2} - \beta^2}\right)\right) = 0.
\end{aligned} \tag{18}$$

It has a non-trivial solution only if its determinant vanishes. Hence we are led to the characteristic equation

$$\begin{aligned}
0 = {} & \alpha^2 m^2 J_m^2(\sqrt{\alpha^2 - \beta^2})\, J_m\left(-\sqrt{\frac{\alpha^4}{\gamma \alpha^2 - \delta^2} - \beta^2}\right) + (\alpha^2 - \beta^2) J'_m(\sqrt{\alpha^2 - \beta^2}) \\
& \cdot (-\beta^2 J'_m(\sqrt{\alpha^2 - \beta^2})\, J_m\left(-\sqrt{\frac{\alpha^4}{\gamma \alpha^2 - \delta^2} - \beta^2}\right) \\
& + \sqrt{\alpha^2 - \beta^2}\, \sqrt{\frac{\alpha^4}{\gamma \alpha^2 - \delta^2} - \beta^2}\, J_m(\sqrt{\alpha^2 - \beta^2})\, J'_m\left(-\sqrt{\frac{\alpha^4}{\gamma \alpha^2 - \delta^2} - \beta^2}\right).
\end{aligned} \tag{19}$$

The number of variables was reduced by introducing the dimensionless expressions

$$\alpha = \sqrt{\sigma R^2/\nu_0}\,, \quad \beta = kR, \quad \gamma = \mu_0/\nu_0, \quad \delta = c_c R/\nu_0. \tag{20}$$

In practical problems, γ and δ are known constants of the fluid and the pipe, e.g. for water $\gamma \approx 3$, $\delta \approx 1.4 \cdot 10^7$ and for air $\gamma \approx 2$, $\delta \approx 2.2 \cdot 10^5$ at normal pressure and room temperature in a pipe with radius $R = 1$ cm [8, p. 171], [9, p. 320]. Furthermore m, the multipolarity of the mode, should be regarded as given. Now it depends whether the decay constant α^2 or the wave number β is provided. The missing value is determined, in both cases, from the characteristic equation (19) by numerical solution. Next, one of the constants a_0, b_0 or c_0 can be chosen, whence the two others may be computed from (18). Finally, returning via (20) to physical units, pressure and velocity fields can be computed from (16) and (17).

In the following I shall provide the time constant α^2 and compute the wave number β, and I will presume, with two important exceptions [cf. Sect. f) and g)], that α^2 is not negative. The reason is that, in order to describe experiments, one would like to solve the "transient problem", where initial values $\boldsymbol{u}(r, \varphi, z, t = 0) = \mathbf{0}$ and boundary values $\boldsymbol{u}(r, \varphi, z = 0, t) = \boldsymbol{w}(r, \varphi, t)$ at the inlet are given, as Laplace transform [10, p. 507 ff.]

$$\boldsymbol{u}(r, \varphi, z, t) = \int_0^\infty \sum_i f_i(\sigma)\, \boldsymbol{u}_i(r, \varphi, z, t)\, \mathrm{d}\sigma. \tag{21}$$

Here only nonnegative values of σ and, because of (20), α^2 are needed. In (21), $\boldsymbol{u}_i(r, \varphi, z, t)$ is one of the velocity fields (17) incorporating the factor $e^{-\sigma t}$ indicative of a Laplace transform. The sum goes over all fields which belong to a fixed σ, and $f_i(\sigma)$ is determined from $\boldsymbol{w}(r, \varphi, t)$.

The question if these Stokes modes are complete remains open. However I assume this since we have solved a four-dimensional problem in space-time and have three separation constants (m, k, σ) at our disposal.

b) Maps of Zeros

For fixed m and α^2, we find infinitely many complex solutions $\beta = \beta_r + i\beta_i$ of the characteristic equation (19). These zeros move as α^2 varies and generate thus trajectories $\beta(\alpha^2)$. The community of all trajectories for fixed m forms a "map of zeros". Even for incompressible flow ($c_c \to \infty$) the maps are so rich that a discussion of this special case seems to be worthwhile. We will consider some modifications due to compressibility in Section g.

The maps of zeros for $m = 0$, 1, 2 and incompressible flow are shown in Figs. 1 and 2. Only $\beta_i \geqq 0$ is

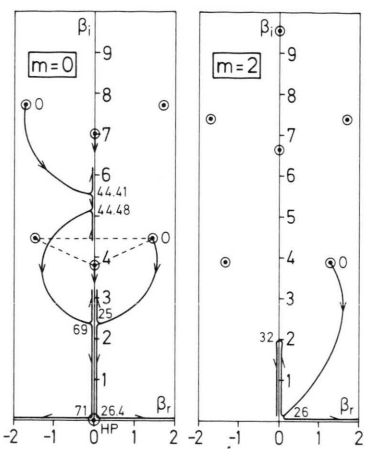

Fig. 1. Maps of zeros for multipolarities $m = 0$ and $m = 2$. Little arcs at turning points and small displacements of the trajectories from the axes are just to clarify the structure of the map. The symmetry with respect to $\pm\beta_r$ was used to compress the information. The meaning of the dashed triangle is explained in Section 3c, and the zero HP at $\beta = 0$ is discussed in Section 3f.

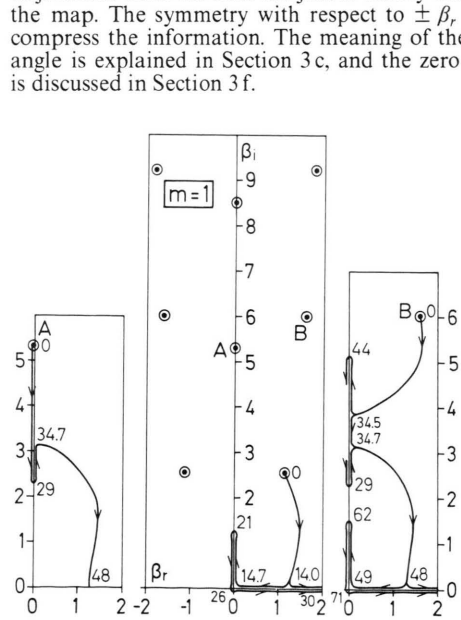

Fig. 2. Map of zeros for multipolarity $m = 1$. In order to demonstrate the entanglement of the trajectories, two of them are depicted separately in the left and right side-figures, viz. those starting from the stationary zeros A and B in the central figure. Most remarkable is the confluence of both trajectories for decay constants $\alpha^2 \gtrsim 34.7$.

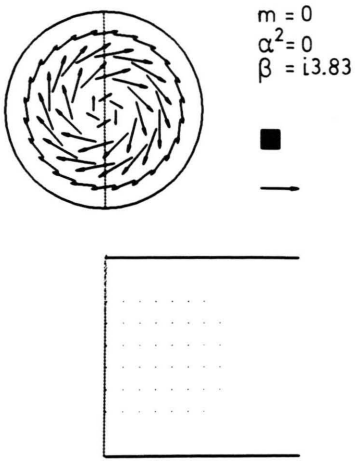

Fig. 3. Central member of the triad corresponding to the triangle in Figure 1. Here and in all following pictures a longitudinal and a transverse cut through the pipe are shown. Their common intersection is indicated by the vertical line. Longitudinally, the pipe begins at the vertical line and extends to the right-hand side without limit. Positive pressures are represented by filled, negative ones by open squares with linear dimensions proportional to the absolute value of the pressure. In (16) p_0 was put equal to zero. The arrows represent the velocities. In the upper right the gauges of velocity and pressure are given. Let the arrow indicate the velocity unit u_0. Then the edge of the single square corresponds to a pressure of u_0 times $\varrho_0 v_0/R$. In the cross sections, arrows and squares were not drawn if they are smaller than one hundredth of the maximum arrow or square, respectively. The specialities of the mode displayed here are the total absence of pressure gradients and the flatness ($\boldsymbol{u}(\boldsymbol{r}, t) \cdot \boldsymbol{e}_z = 0$) of the current.

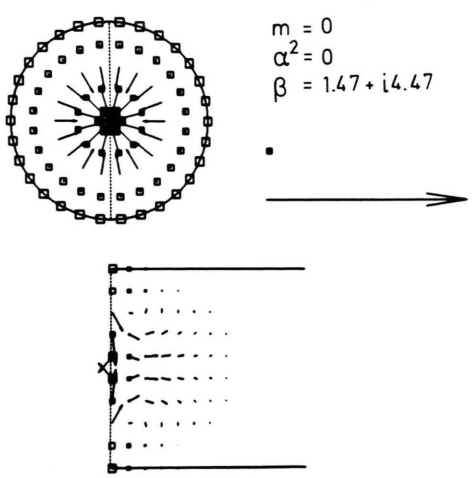

Fig. 4. "Right" member of the triad (cf. the triangle in Figure 1).

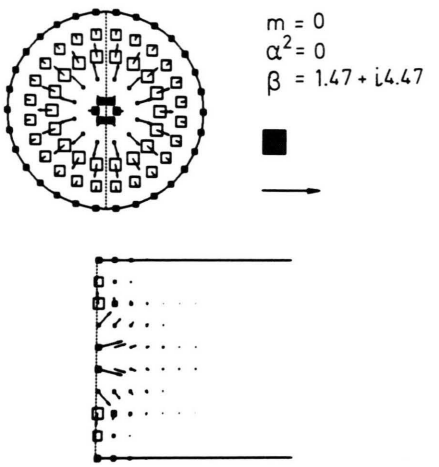

Fig. 5. "Left" member of the triad (cf. the triangle in Figure 1). Instead of taking the right and left zeros in Fig. 1 or forming suitable linear combinations, it amounts to the same to stick to the right zero and to take first the real parts (Fig. 4) and second the imaginary parts (here) of the expressions in (16) and (17). This follows from the fact that the complex conjugate $\bar{\beta}$ solves the characteristic equation (19) if β does so, provided that all other parameters in (19) are real.

displayed because $\beta_i < 0$ gives no new information: If β is a zero of the characteristic equation (19), then the same is true for $-\beta$. Physically, $\beta_i \geqq 0$ means that we consider a semi-infinite pipe $0 \leqq z < \infty$ with its mouth at $z = 0$.

The zeros for stationary modes, which are obtained from (19) by letting $\alpha^2 \to 0$, are visualized by surrounding circles. Each of these dots can be considered as a starting point of a trajectory as α^2 increases. For certain values of α^2 the trajectory bifurcates or turns backwards. To such singular points the respective values of α^2 are affixed in small numerals. Maps of zeros for multipolarities larger than 2 resemble the $m = 2$ map.

c) Ternary Structure of the Stokes Modes

It was pointed out in Sect. 3a that generally *three* independent functions are needed to cover three boundary conditions. And still the boundary conditions at the mouth have to be satisfied. The trinity must show up also in the modes. A typical triad is indicated by the triangle in Figure 1. The corresponding currents are displayed in Figs. 3, 4, and 5. The linear independence of these modes in particular at the mouth of the pipe is easily seen. Their common property is that they have no nodes,

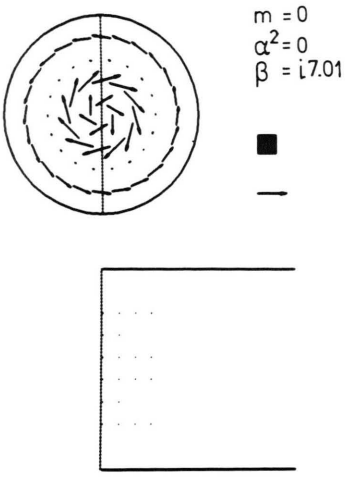

Fig. 6. A higher central mode (cf. Figure 1). Similar as in Fig. 3 we have no pressure gradients at all and a completely flat current.

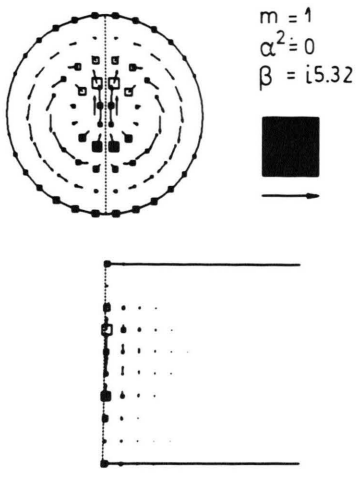

Fig. 7. First mode with multipolarity $m = 1$ (cf. Figure 2).

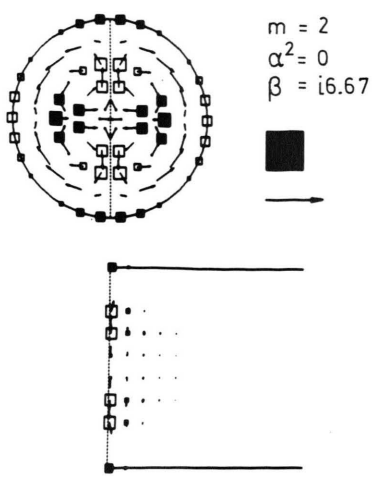

Fig. 8. Multipolarity $m = 2$ (cf. Figure 1). The four sectors in the cross section will be noted. They should be compared with the two sectors in Fig. 7 and the single sector in Figure 3.

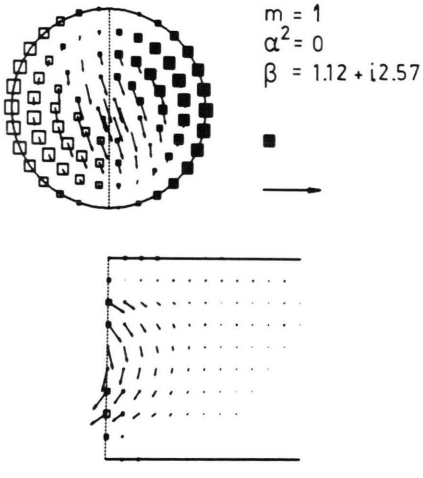

Fig. 9. Stationary mode as starting point for the only depicted trajectory in the central part of Figure 2.

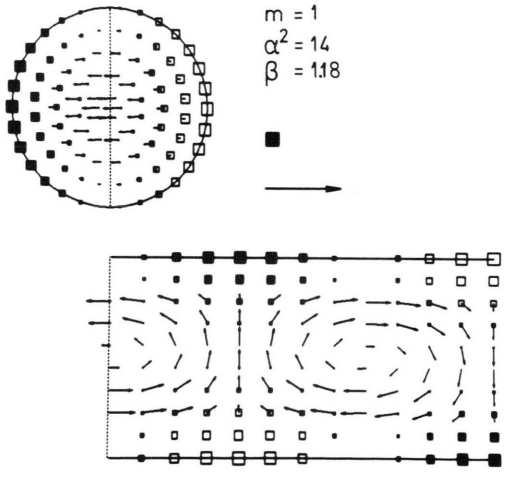

Fig. 10. First breakthrough mode. Of all breakthrough modes this is the one with smallest internal damping (cf. Section 4).

neither axial (r direction) nor azimuthal ones (φ direction).

Looking now for higher and higher triads, i.e. looking for larger and larger β_i, we find very much the same phenomenon as with vibrations of a membrane: For fixed multipolarity we obtain more and more radial surface of nodes. This change is illustrated by Figure 6. If the order of a triad is kept but the multipolarity increased, more and more azimuthal node surfaces arise. This is seen in Figs. 3, 7, and 8.

d) Walking along a Trajectory

Having understood the structure of the Stokes modes for $\alpha^2 \to 0$, one now might wonder how the modes look like when α^2 grows. This is exemplified for the trajectory starting from $\beta \approx 1.1 + i\,2.6$ for $m = 1$ (cf. Figure 2). Its current for $\alpha^2 \to 0$ is shown

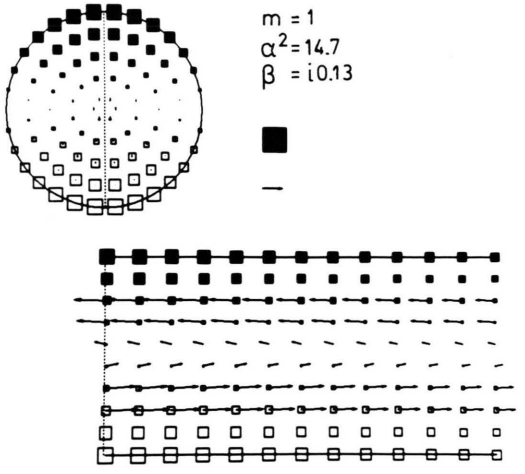

Fig. 11. Nearly an exact solution (cf. Section 3e) of the Navier-Stokes equations. The imperfections are $\beta_i > 0$ instead $\beta = 0$ and consequently a slightly nonparallel flow as well as a decreasing pressure in the direction of the pipe.

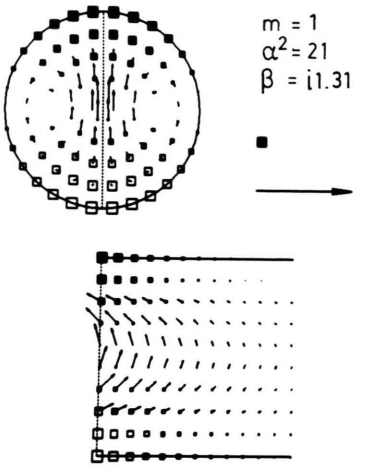

Fig. 12. Last member of the series starting with Figure 9. The picture seems similar to Fig. 7, but this current has a deeper penetration, and the relation between flow and pressure fields is just opposite.

in Figure 9, the most remarkable property being the small depth of penetration into the pipe. Apart from the Hagen-Poiseuille mode to be discussed in Sect. f this is the fate of all stationary Stokes modes: A flow is induced by the boundary conditions at the mouth, but, as long as the regime stays stationary, the perturbation remains localized (see also Figures 1 – 8). The feature alters as soon as α^2 gets positive. β_i decreases then, as seen in Fig. 2, and this means, according to the definition of β as dimensionless wave number, that the penetration increases. The metamorphosis is accomplished when the trajectory touches the real axis ($\beta \approx 1.2$, $\alpha^2 \approx 14.0$). The respective current is depicted in Figure 10. A perturbation at the mouth is now propagated through the entire semi-infinite pipe. At the same time the trajectory branches off. We will follow the left-hand branch since it is the more interesting. Arriving at $\beta = 0$, $\alpha^2 \approx 14.7$ the corresponding mode is entirely straight (see Fig. 11), the pipe seems to be divided into two halves, each of them guiding exclusively backward or forward flow. At $\beta = 0$ there occurs another branching, and a new metamorphosis sets in: The straight mode transforms into a completely flat one; this means that the velocity field has no z component. We follow the branch moving upwards in Figure 2. The mode of the turning point at $\beta \approx i\,1.3$, $\alpha \approx 21$ is shown in Fig. 12, where the heart-like flow pattern is not yet entirely flat. When the trajectory returns at $\alpha^2 \approx 26$ to $\beta = 0$, the mode again breaks through the pipe but now it is flat. It retains its heart-like face. Finally, with $\beta_i = 0$, β_r increasing, the mode gets more and more cells in a similar manner as indicated in the longitudinal section of Figure 10. The transverse cross section, however, is different.

A common feature of all trajectories is that they approach the real axis $\beta_i = 0$ if α^2 gets large enough. Namely for the incompressible liquid

$$0 = J_m(\sqrt{\alpha^2 - \beta^2}) \tag{22}$$

can be read from (19) to be the characteristic equation for $\alpha^2 \to \infty$ (cf. also Section g). It has only real solutions $\beta = \beta_r$ for $\alpha^2 \to \infty$ because $J_m(z)$ possesses only real zeros. The appropriate physical interpretation that all modes, which *decay* fast enough, propagate through the pipe has a counterpart in electrodynamics [11, p. 293, p. 315 ff.] where all waves *oscillating* sufficiently fast behave in quite the same way. The details, however, are very different. For example, numerical inspection of the characteristic equation (19) for imaginary α^2 and $\delta \to \infty$ shows that there are almost no oscillating modes in incompressible hydrodynamics which break through, the only exception being those modes that are connected with the Hagen-Poiseuille zero (HP) in

Figure 1. They will be discussed in the next but one section.

e) Exact Solutions

If one searches for solutions of the Stokes problem which do not depend on z, one has to put $\beta = 0$ in (18) and to distinguish between two cases, a_0 arbitrary and $a_0 = 0$. The results are collected in Table 1. It is seen from the table and from (17) that the velocity fields which obey the characteristic equation $J_0'(\alpha) = 0$ have just a component in φ direction whereas the only component corresponding to $J_m(\alpha) = 0$ points along the z axis. All velocity fields of the second class have thus the form

$$\boldsymbol{u}(\boldsymbol{r}, t) = \boldsymbol{e}_z f(r, \varphi, t). \tag{22}$$

$f(r, \varphi, t)$ is some function independent of z. For flows of the type (22) the convective term $(\boldsymbol{u}\nabla)\boldsymbol{u}$ in (4) vanishes. If incompressibility is assumed, the neglect of this term is the only effect of linearization, and therefore all Stokes modes with the additional property (22) are exact solutions of the Navier-Stokes equations (1) and (2) with $\varrho = \varrho_0$, $\eta = \eta_0$, $\lambda = \lambda_0$. An example for such an exact solution is indicated in Figure 11.

Table 1. Conditions of solvability of the linear system (18) for $\beta = 0$ and $\delta \to \infty$ (incompressible fluid). The second line contains the simplified characteristic equation for the decay constant α^2 and the three lines below the allowed values of the coefficients a_0, b_0 and c_0. For the multipolarity $m = 0$ we have an alternative. For $m = 1, 2, \ldots$ only the right column applies.

$m = 0$	$m = 0, 1, 2, \ldots$
$J_0'(\alpha) = 0$	$J_m(\alpha) = 0$
a_0 arbitrary	$a_0 = 0$
$b_0 = 0$	b_0 arbitrary
c_0 arbitrary	c_0 arbitrary

Table 2. Similar to Table 1, but now for the linear system (25). There is again an alternative for $m = 0$. Note that the first case needs no characteristic equation at all.

$m = 0$	$m = 0$	$m = 1, 2, 3, \ldots$
α arbitrary	$J_0'(\alpha) = 0$	$J_m(\alpha) = 0$
$a_1 = 0$	a_1 arbitrary	a_1 arbitrary
b_1 arbitrary	b_1 arbitrary	b_1 arbitrary
$c_1 = -(b_1/R^2)$ $\cdot \alpha^2 J_0(\alpha)$	$c_1 = -(b_1/R^2)$ $\cdot \alpha^2 J_0(\alpha)$	$c_1 = -(a_1/m)$ $\cdot i\alpha J_m'(\alpha)$

For the multipolarity $m \neq 0$, the exact solutions can occur only at certain countable values α_1^2, α_2^2, $\alpha_3^2, \ldots$ of decay constants, namely if a trajectory visits the origin $\beta = 0$ in the map of zeros. For $m = 0$, however, there are moreover exact solutions for all complex values of α^2 as we will see in the next section. They are all hidden in the Hagen-Poiseuille zero (HP) of Figure 1. HP is therefore a zero of supercountable multiplicity.

f) The Hagen-Poiseuille Zero

Starting from the potentials (15) and putting $\beta = 0$ in the boundary conditions (18) irrevocably delivers the results of Table 1, i.e. countable sets of decay constants α^2. We may, however, form linear combinations with potentials obtained from (15) by the change from k to $-k$. The requirement of a *definite parity* $z \leftrightarrow -z$ *of the velocity field* pins us down to put (with $c_c \to \infty$)

$$\begin{aligned}
\boldsymbol{v}\, a(r, \varphi, z, t) &= \boldsymbol{e}_z a_1 J_m\left(\sqrt{\frac{\sigma}{\nu_0} - k^2}\, r\right) \\
&\quad \cdot e^{im\varphi} \frac{\sin k z}{k} e^{-\sigma t}, \\
\boldsymbol{v}\, b(r, \varphi, z, t) &= \boldsymbol{e}_z b_1 J_m\left(\sqrt{\frac{\sigma}{\nu_0} - k^2}\, r\right) \\
&\quad \cdot e^{im\varphi} \cos k z\, e^{-\sigma t}, \\
c(r, \varphi, z, t) &= c_1 J_m(-ikr)\, e^{im\varphi} \frac{\sin k z}{k} e^{-\sigma t}.
\end{aligned} \tag{23}$$

The constants a_1, b_1, c_1 were introduced in a way to make the limiting process $k \to 0$ as easy as possible:

$$\begin{aligned}
\boldsymbol{v}\, a(r, \varphi, z, t) &= \boldsymbol{e}_z a_1 J_m\left(\sqrt{\frac{\sigma}{\nu_0}}\, r\right) e^{im\varphi} z\, e^{-\sigma t}, \\
\boldsymbol{v}\, b(r, \varphi, t) &= \boldsymbol{e}_z b_1 J_m\left(\sqrt{\frac{\sigma}{\nu_0}}\, r\right) e^{im\varphi} e^{-\sigma t}, \\
c(z, t) &= c_1 \delta_{m0} z\, e^{-\sigma t}.
\end{aligned} \tag{24}$$

The boundary conditions $\boldsymbol{u}(r = R, \varphi, z, t) = \boldsymbol{0}$ lead now to

$$\begin{aligned}
&\frac{a_1}{R}(i m J_m(\alpha)) = 0, \\
&\frac{a_1}{R}(-\alpha J_m'(\alpha)) + \frac{c_1}{R}(i m) = 0, \\
&\frac{b_1}{R^2}(\alpha^2 J_m(\alpha)) + \frac{c_1}{R}(R \delta_{m0}) = 0
\end{aligned} \tag{25}$$

as a substitute of (18). This system allows *three* types of solutions, which are presented in Table 2.

The peculiar discovery is the first column in Table 2, namely that there are solutions for all complex values of α. Moreover, the respective modes turn out to be all exact solutions of the Navier-Stokes equations for incompressible flow since they have the property (22). Explicitly, the velocity fields are found with (9) to be

$$\boldsymbol{u}(r,t) = \boldsymbol{e}_z b_1 \frac{\sigma}{\nu_0}\left(J_0\left(\sqrt{\frac{\sigma}{\nu_0}}\, r\right) - J_0\left(\sqrt{\frac{\sigma}{\nu_0}}\, R\right)\right) e^{-\sigma t} \tag{26}$$

and the pressure according to (10)

$$p(z,t) = p_0 - \varrho_0 b_1 \frac{\sigma^2}{\nu_0} J_0\left(\sqrt{\frac{\sigma}{\nu_0}}\, R\right) z\, e^{-\sigma t} \tag{27}$$

with an arbitrary constant b_1 and arbitrary complex σ. The solution (26, 27) contains the familiar Hagen-Poiseuille flow. We only let $\sigma \to 0$, identify

$$u_0 = b_1 \left(\frac{\sigma R}{2\nu_0}\right)^2 \tag{28}$$

as the velocity in the center of the pipe and find

$$\boldsymbol{u}(r) = \boldsymbol{e}_z u_0 (1 - r^2/R^2), \tag{29}$$

$$p(z) = p_0 - 4\varrho_0 \nu_0 u_0 / R^2 \cdot z\,. \tag{30}$$

Both results, (26, 27) and (29, 30), are well-known [12], [13], [14]. The present derivation, however, is remarkable for a principal reason: It is sometimes suggested (see e.g. [15, Sect. 7]) that a stationary Stokes flow cannot be derived from the time-dependent modes, and a superficial application of the theorem in Chapt. 2 to the Hagen-Poiseuille flow (29, 30) seems to confirm this point of view. Nevertheless we have seen that it takes just a judicious limiting process to overcome the difficulty.

g) Propagation of Sound

The theory of sound in ducts is a well-treated subject [16, pp. 44–61] which becomes difficult when friction of any kind is included. Most advanced seems to be the analysis by Fritsche [17] who computed axially symmetrical modes in a cylindrical resonator. But even for axial symmetry only that limiting case was investigated where deviations from the ideal theory of sound can be approximated by first terms of power series. The present section is to clarify the connection of the formulae given in Sect. a with the "usual theory of sound".

First the term "usual theory of sound" shall be defined. Since sound is associated with longitudinal waves, one is inclined to describe its velocity and pressure fields by the scalar potential $c(\boldsymbol{r}, t)$ alone (cf. (9) and (10)). In (17) and (18) we only have to cross out the first two columns on the right-hand side. As a price for this simplification we must be content with a less realistic boundary condition, viz. $u_r(r = R, \varphi, z, t) = 0$, meaning that only the radial component of the velocity yield vanishes instead of the velocity field itself. This replaces (19) as characteristic equation by

$$0 = J'_m\left(-\sqrt{\frac{\alpha^4}{\gamma\alpha^2 - \delta^2} - \beta^2}\right), \tag{31}$$

which also is obtained directly from (19) for $|\alpha^2| \to \infty$. Let us for a moment neglect the damping term with γ and denote by z_n the nth zero of the equation $J'_m(z_n) = 0$. Then (31) may be rewritten as

$$\beta = \pm\sqrt{-\alpha^4/\delta^2 - z_n^2}\,, \tag{32}$$

which shows that propagation of sound in a duct is possible only for oscillatory perturbations (α^2 imaginary) if moreover a certain cutoff frequency

$$|\alpha^2| \geqq z_n \delta \tag{33}$$

is exceeded. The result is completely analogous to the electromagnetic case but opposite to the behaviour of incompressible fluids (see Sect. d). Thus, to observe the zeros of sound modes, we have to draw maps of zeros for *imaginary* α^2 and to look for trajectories which start at $\beta = \pm i z_n$, approach $\beta = 0$ for increasing $|\alpha^2|$ and finally bifurcate at $\beta = 0$ to proceed henceforth on the real β axis. It is not a trivial question to reconcile these motions of a single zero with the ternary structure of Stokes modes as discussed in Section c.

The answer based on numerical solution of the characteristic equation (19) is given in Figure 13. This map of zeros is to be compared with Fig. 1, the main difference being that in Fig. 1 α^2 is a nonnegative *real* number. For incompressible flow the stationary central zero at $\beta \approx i\,3.8$ and the right-hand side zero at $\beta \approx 1.5 + i\,4.5$ move to the upper right when the frequency grows. This corresponds to waves running into the pipe which penetrate the less the shorter their wavelength is. Such a behaviour is

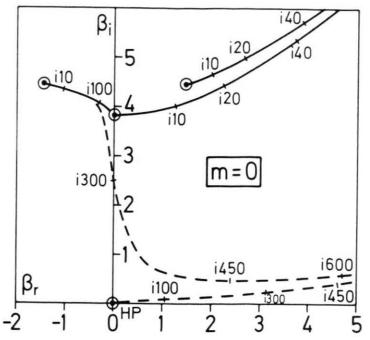

Fig. 13. Map of zeros for multipolarity $m=0$. The small numbers at the trajectories give the respective value of α^2. Drawn lines show trajectories related to incompressible flow ($\delta \to \infty$), whereas broken lines refer to compressible modes for $\gamma=2$, $\delta=100$ (cf. (20)). The order of magnitude of $\gamma=2$ is correct for many substances, but $\delta=100$ corresponds just to a highly viscous oil. If we had taken $\delta \approx 10^6$ to describe water or air (see Sect. a), we had found compressible trajectories pressing themselves so close to the β_r and β_i axes that it were difficult to distinguish them. The map of zero for negative imaginary α^2 is obtained from this substituting β_r by $-\beta_r$ (see (19) for a proof).

known from Stokes boundary layers [15]. The left-hand side trajectory starting from $\beta \approx -1.5 + i\,4.5$ converges for $|\alpha^2| \to \infty$ toward the stationary central zero and exhibits thus an unexpected trait. Its physical significance becomes clear if compressibility is allowed. For compressible flow the central and right-hand side trajectories coincide, within the limits of the figure, with their incompressible analogues. The left-hand side trajectory, however, departs at $\alpha^2 \approx i\,100$ from its incompressible counterpart. It continues in the way approximately described by (32). Because of viscosity a complete breakthrough is never attained. There is only a maximum of penetration at $\alpha^2 \approx i\,450$. This fact illuminates the singular nature of incompressible fluids as compared with sound and electromagnetic fields: Incompressible flow can break through even if viscosity is present (cf. Section d).

A similar remark applies to the Hagen-Poiseuille zero which looses its unique properties and describes just a damped sound mode as soon as compressibility is switched on (see Figure 13).

We can understand the number $\alpha^2 \approx i\,100$ of departure by the observation that deviations from incompressibility must become essential if in (31)

$$\left| \frac{\alpha^4}{\gamma\,\alpha^2 - \delta^2} \right| \approx |\beta|^2. \tag{34}$$

But this means

$$|\alpha^2| \approx \delta\,|\beta| \tag{35}$$

since usually $\gamma \ll \delta$ and $|\beta|$ should be of order one for the first deviation from incompressibility. An even cruder estimate is $|\alpha^2| \approx \delta$, and this gives $|\alpha^2| \approx 100$ in the present case.

When we translate the estimate (35) by (20) to physical units, we find

$$|\sigma| \approx c_c\,|k|, \tag{36}$$

which is the trademark for the propagation of sound. Translation of (31) leads to

$$\sigma = \mu_0 \left(k^2 + \left(\frac{z_n}{R} \right)^2 \right) \pm i \sqrt{c_c^2 \left(k^2 + \left(\frac{z_n}{R} \right)^2 \right) - \frac{\mu_0^2}{4} \left(k^2 + \left(\frac{z_n}{R} \right)^2 \right)^2} \tag{37}$$

which shows the damping (first term) and frequency decrease (root) due to bulk viscosity μ_0. One must, however, not believe that (37) gives the first approximation regarding friction because the proper boundary conditions $\boldsymbol{u}(r=R, z, \varphi, t) = \mathbf{0}$ induce terms containing v_0 which are not less important than those in (37).

A related problem, namely how sound is "hidden" in the modes of a compressible but inviscid jet, was solved only quite recently [18].

In a certain aspect Fritsche's work [17] is more advanced than the theory developed here since he takes heat conduction into account. Furthermore, diffusion and the internal relaxation of the gas or the fluid should be considered if comparison with accurate measurements is intended [8]. All these extensions can be done with methods presented in the appendix and produce not more difficulties than a larger amount of writing.

4. Speculations

Although sound measurements in a tube are important enough for the information they give on the interaction between molecules, the reason for the present work was to open a new approach for the study of the onset of turbulence. Three paths might be most rewarding.

a) The most promising ansatz to explain the onset of turbulence in a pipe was made by Mackrodt [19]. He added to the Hagen-Poiseuille current a rotation

of the whole pipe about its axis. He showed, theoretically and experimentally, that the combined flow becomes unstable when a certain angular velocity is transgressed. An objection against this work may be that normally pipes do not rotate but still permit a transition to turbulence. Mackrodt goes on to argue: Normally the rotation is induced at the inlet and concerns just the fluid but not the walls. For this case, however, his combined flow does not satisfy the proper boundary conditions. The present work gives enough modes to model a Hagen-Poiseuille flow plus an internal rotation fulfilling the correct boundary conditions (see Figs. 3 and 6).

b) Mackrodt's basic idea to search for an onset of turbulence not in the vicinity of the Hagen-Poiseuille flow is convincing because it agrees with the experimental finding of a suppressed transition when one struggles for clean preparation of Hagen-Poiseuille. To take a rotation as addendum is nevertheless not compelling. The present work gives a great stock of exact solutions remaining exact if they are combined with Hagen-Poiseuille (compare Sects. 2e and f). Moreover these solutions need pressure patterns at the mouth which may occur quite naturally in nearly every experiment (see e.g. Figure 11). The accompanying pressure gradients are amazingly small. For our standard pipe ($\nu_0 = 0.01\ \mathrm{cm^2\,s^{-1}}$, $R = 1$ cm, velocities $\approx 10\ \mathrm{cm\,s^{-1}}$) we find from Fig. 11 1 μbar $\mathrm{cm^{-1}}$ as the order of magnitude. The next step one has to perform is to linearize the Navier-Stokes equations about these exact solutions. v. Kerczek and Davis have done the corresponding step for a simpler system [15]. One obtains linear partial differential equations with time- and space-dependent coefficients. Today it should be possible to solve these equations by numerical means. The modes of Sect. 3a can serve as a basis to simplify the numerical analysis.

c) The solutions of the non-linear Navier-Stokes system (1)–(3) can be sought as a series in terms of the modes of Section 3a. The ansatz transforms the non-linear partial differential equations into a set of non-linear ordinary differential equations for the time-dependent amplitudes in the series. The procedure is the same which led Saltzman [20] and Lorenz [21] to the discovery of the three famous differential equations for the plane Bénard system. The pipe, however, is more typical for the generation of turbulence since the propelling energy enters the system as motion of the fluid and not just as heat.

Table 3. Smallest possible decay constants α^2 for breakthrough at $\beta = 0$ of incompressible currents through a semi-infinite pipe. By comparison with Tables 1 and 2 it may be seen that all α values are zeros of $J_m(\alpha)$ or $J_0'(\alpha)$ belonging to the multipolarities m printed in the first line. To give some feeling for the time scale involved, α^2 was converted into decay times $\sigma^{-1} = R^2/\nu_0 \cdot \alpha^2$ (cf. (20)) for water ($\nu_0 = 0.01\ \mathrm{cm^2\,s^{-1}}$) in a pipe with radius $R = 1$ cm.

m	0, 1	0, 1, 2	1, 2, 3	0, 1	0, 1, 2
α^2	14.6820	26.3746	40.7064	49.2185	70.8499
σ^{-1}/s	6.8	3.8	2.5	2.0	1.4

The above-mentioned series expansion would be useful for discussion only if a few terms were sufficient to describe most of the physics. It is tempting to speculate on the relevance of the various modes starting from the material given in Sects. 3c to f. The Hagen-Poiseuille flow is indispensable since it is the engine of the process. Other relevant modes should have a small internal damping, expressed by a small value of α^2, and they should penetrate deeply into the pipe. The latter condition is related to the fact that the strength of the coupling between the modes is determined by overlap integrals between the modes, similar to the matrix elements in quantum mechanics. A spatially strongly decaying mode is confined to a small part of the pipe and can thus not interact effectively with other modes. The smallest values of α^2 for which $\beta = 0$ is reached are collected in Table 3. Surprisingly modes with multipolarity $m = 1$ are favoured. In addition it must be stressed that the lowest value of α^2 ($\alpha^2 \approx 14.0$), for which breakthrough is reached, comes from an $m = 1$ mode with non-zero wave number β. It is shown in Figure 10. $m = 1$ seems to be the only multipolarity which manages the first breakthrough at $\beta \neq 0$. The other noticeable thing are perhaps the long decay times given in Table 3.

Appendix

Here the theorem enunciated in Sect. 2 will be proven. In advance two remarks might be useful.

No attempt will be made to prove that *all* solutions of the original problem (7–8) can be found in the manner the theorem indicates. However, we have three scalar quantities $a(\boldsymbol{r}, t)$, $b(\boldsymbol{r}, t)$ at our

disposal and one independent vector field $\boldsymbol{u}(\boldsymbol{r}, t)$ in the original problem as the pressure $p(\boldsymbol{r}, t)$ is determined from $\boldsymbol{u}(\boldsymbol{r}, t)$ by (7) or (8) up to a meaningless function depending only on time. Moreover, for somewhat simpler problems in the theory of elasticity proofs of completeness for similar representation theorems exist [22, pp. 232–238], [23], and this gives some confidence in the like completeness of the present representation.

The basic idea of the derivation of the theorem is to take the representation formula (9) for granted and to construct from it the differential equations (11)–(13) as well as the missing representation formula (10). The same procedure can be easily applied to other problems of mathematical physics involving vector fields [24].

The proof proceeds as follows: For the beginning we put $b(\boldsymbol{r}, t) = 0$ and insert formula (9) into (7)

$$\begin{aligned}&\partial_t \nabla x\,(\boldsymbol{v}\, a(\boldsymbol{r}, t)) + \partial_t c(\boldsymbol{r}, t)\\ &\quad = -\nabla p(\boldsymbol{r}, t)/\varrho_0 + \mu_0 \nabla(\nabla^2 c(\boldsymbol{r}, t))\\ &\quad\quad - \nu_0 \nabla x\,(\nabla x\,(\nabla x\,(\boldsymbol{v}\, a(\boldsymbol{r}, t)))).\end{aligned} \tag{A. 1}$$

Separating transverse and longitudinal parts yields two sufficient equations:

$$\nabla x\,(\partial_t \boldsymbol{v}\, a(\boldsymbol{r}, t)) = -\nu_0 \nabla x\,(\nabla x\,(\nabla x\,(\boldsymbol{v}\, a(\boldsymbol{r}, t)))), \tag{A. 2}$$

$$\nabla \partial_t c(\boldsymbol{r}, t) = -\nabla p(\boldsymbol{r}, t)/\varrho_0 + \mu_0 \nabla(\nabla^2 c(\boldsymbol{r}, t)). \tag{A. 3}$$

Integration of the latter equation with respect to $\boldsymbol{r}$ leads to the representation (10). If both (9) and (10) are inserted into (8), we find the differential equation (13).

Equation (A. 2) can be written as

$$\nabla x\,(\partial_t (\boldsymbol{v}\, a(\boldsymbol{r}, t)) - \nu_0 \nabla^2 (\boldsymbol{v}\, a(\boldsymbol{r}, t))) = \boldsymbol{0}. \tag{A. 4}$$

The only way to transform this into a scalar equation for $a(\boldsymbol{r}, t)$, which is independent of $\boldsymbol{v}(\boldsymbol{r}, t)$, is to pull the supporting vector field $\boldsymbol{v}$ through the laplacian. In cartesian coordinates the second term in (A. 4) may be written as

$$\begin{aligned}\nabla^2 (v_x\, a(\boldsymbol{r}, t)) &= a(\boldsymbol{r}, t)\, \nabla^2 v_x + 2(\nabla v_x)(\nabla a(\boldsymbol{r}, t))\\ &\quad + v_x \nabla^2 a(\boldsymbol{r}, t),\\ \nabla^2 (v_y\, a(\boldsymbol{r}, t)) &= a(\boldsymbol{r}, t)\, \nabla^2 v_y + 2(\nabla v_y)(\nabla a(\boldsymbol{r}, t))\\ &\quad + v_y \nabla^2 a(\boldsymbol{r}, t),\\ \nabla^2 (v_z\, a(\boldsymbol{r}, t)) &= a(\boldsymbol{r}, t)\, \nabla^2 v_z + 2(\nabla v_z)(\nabla a(\boldsymbol{r}, t))\\ &\quad + v_z \nabla^2 a(\boldsymbol{r}, t)\end{aligned} \tag{A. 5}$$

with $\boldsymbol{v} = v_x \boldsymbol{e}_x + v_y \boldsymbol{e}_y + v_z \boldsymbol{e}_z$ and the cartesian unit vectors $\boldsymbol{e}_x$, $\boldsymbol{e}_y$, $\boldsymbol{e}_z$. Only the last terms on the right-hand sides of (A. 5) are welcome. The other terms jeopardize the project of obtaining an equation for $a(\boldsymbol{r}, t)$ alone because they couple $a(\boldsymbol{r}, t)$ with $\boldsymbol{v}$. Nevertheless it is not correct to demand that these terms should vanish completely. A gradient may remain since there is still a curl in front of (A. 4) which would kill it. For arbitrary $a(\boldsymbol{r}, t)$, the only way to produce a gradient in (A. 5) is to stipulate

$$\nabla v_x = \boldsymbol{e}_x v_1, \quad \nabla v_y = \boldsymbol{e}_y v_1, \quad \nabla v_z = \boldsymbol{e}_z v_1 \tag{A. 6}$$

if v_1 denotes a scalar not depending on $\boldsymbol{r}$. These equations may be integrated at once:

$$\boldsymbol{v} = \boldsymbol{v}_0 + v_1 \boldsymbol{r}. \tag{A. 7}$$

Also the vector $\boldsymbol{v}_0$ must not depend on $\boldsymbol{r}$. Simultaneously (A. 7) fulfills $\nabla^2 \boldsymbol{v} = \boldsymbol{0}$ so that there are now no disturbing non-gradient terms on the right-hand side (A. 5). Up to now it seems as if $\boldsymbol{v}_0$ and v_1 might still depend on time. This however is not possible because pulling $\boldsymbol{v}$ through the operator ∂_t would produce the non-gradient term $a(\boldsymbol{r}, t)\, \partial_t \boldsymbol{v}$ in (A. 4). These remarks explain the origin of (14).

With (14), (A. 4) becomes

$$\nabla x\,(\boldsymbol{v}\,(\partial_t a(\boldsymbol{r}, t) - \nu_0 \nabla^2 a(\boldsymbol{r}, t))) = \boldsymbol{0}. \tag{A. 8}$$

Integration over some surface in ordinary space and application of Stokes' theorem gives

$$\oint \mathrm{d}\boldsymbol{s} \cdot \boldsymbol{v}\,(\partial_t a(\boldsymbol{r}, t) - \nu_0 \nabla^2 a(\boldsymbol{r}, t)) = 0, \tag{A. 9}$$

which implies a simple connection of the domain in which the solution is sought. Since the surface was arbitrarily chosen, we find from (A. 9)

$$\partial_t a(\boldsymbol{r}, t) - \nu_0 \nabla^2 a(\boldsymbol{r}, t) = f(\cdot, t) \tag{A. 10}$$

with a free function

$$f(\cdot, t) = \begin{cases} f(|\boldsymbol{v}|\, t) & \text{if } v_1 \neq 0 \\ f(\boldsymbol{v}_0 \boldsymbol{r}, t) & \text{else,} \end{cases} \tag{A. 11}$$

i.e. at fixed time the function $f(\cdot, t)$ must vary only in the direction of the supporting vector field.

There is no loss of generality if we assume $f(\cdot, t) = 0$. For we may introduce a new function $\tilde{a}(\boldsymbol{r}, t)$ by a "gauge transform"

$$\tilde{a}(\boldsymbol{r}, t) = a(\boldsymbol{r}, t) - \Lambda(\cdot, t), \tag{A. 12}$$

$$\Lambda(\cdot, t) = \begin{cases} \Lambda(|\boldsymbol{v}|, t) & \text{if } v_1 \neq 0 \\ \Lambda(\boldsymbol{v}_0 \boldsymbol{r}, t) & \text{else,} \end{cases} \tag{A. 13}$$

which does exactly the same job in the representation formulae (9) and (10) as $a(\boldsymbol{r}, t)$. $\Lambda(\cdot, t)$ can be

chosen to satisfy the inhomogeneous equation

$$\partial_t \Lambda(\cdot, t) - \nu_0 \nabla^2 \Lambda(\cdot, t) = f(\cdot, t). \qquad \text{(A. 14)}$$

Subtraction of this equation from (A. 10) yields a homogeneous equation for $\tilde{a}(\boldsymbol{r}, t)$, i.e. (11). The present gauge consisting in the choice of a definite supporting vector field and in putting $f(\cdot, t) = 0$ is in so far advantageous over the differential gauges known in electrodynamics as the Coulomb and the Lorentz gauge since our gauge permits complete decoupling of the differential equations whereas the differential gauges generally do not.

Finally we abandon the restriction $b(\boldsymbol{r}, t) = 0$: If $a(\boldsymbol{r}, t)$ satisfies (A. 2) with a triple curl on the right-hand side, $b(\boldsymbol{r}, t)$ has to fulfill a similar equation with quadruple curl, as is obvious from its introduction by the representation (9). However, if $\boldsymbol{v}$ has the form (14) and $b(\boldsymbol{r}, t)$ satisfies the differential equation (12), the equation with triple curl and all the more with quadruple curl are indeed fulfilled.

Acknowledgement

I am grateful to Prof. S. Grossmann for many discussions, his careful reading of the manuscript and the ensuing valuable suggestions.

[1] P. Drazin and W. Reid, Hydrodynamic Stability, University Press Cambridge 1981.
[2] H. Schlichting, Grenzschicht-Theorie, Verlag G. Braun, Karlsruhe 1982.
[3] T. Sarpkaya, J. Basic Engineering (Trans. ASME. SER. D.) **88,** 589 (1966).
[4] P. K. Sen, D. Venkateswarlu, and S. Maji, J. Fluid Mech. **158,** 289 (1985) and references therein.
[5] M. Lessen, S. G. Sadler, and T. Y. Liu, Phys. Fluids **11,** 1404 (1968).
[6] H. Salwen and C. E. Grosch, J. Fluid Mech. **54,** 93 (1972).
[7] P. M. Morse and H. Feshbach, Methods of Theoretical Physics, Parts I and II, McGraw-Hill Book Company, New York 1953.
[8] H. O. Kneser, Schallabsorption und -dispersion in Gasen, in: Handbuch der Physik, ed. S. Flügge, Vol. XI/1, Springer-Verlag, Berlin 1961.
[9] D. Sette, Dispersion and Absorption of Sound Waves in Liquids and Mixtures of Liquids, in: Handbuch der Physik, ed. S. Flügge, Vol. XI/1, Springer-Verlag, Berlin 1961.
[10] R. Courant and D. Hilbert, Methods of Mathematical Physics, Vol. II, Interscience Publishers, New York 1962.
[11] F. E. Borgnis and C. H. Papas, Electromagnetic Waveguides and Resonators, in: Handbuch der Physik, ed. S. Flügge, Vol. XVI, Springer-Verlag, Berlin 1958.
[12] Th. Sexl, Z. Phys. **61,** 349 (1930).
[13] F. Szymansky, J. math. pures appliquées (9) **11,** 67 (1932).
[14] S. Uchida, Z. Angew. Math. Phys. **7,** 403 (1956).
[15] C. v. Kerczek and S. H. Davis, J. Fluid Mech. **62,** 753 (1974).
[16] P. M. Morse and K. U. Ingard, Linear Acoustic Theory, in: Handbuch der Physik, ed. S. Flügge, Vol. XI/1, Springer-Verlag, Berlin 1961.
[17] L. Fritsche, Der akustische Zylinderresonator, Dissertation, Universität Stuttgart 1958.
[18] A. Müller and S. Grossmann, Z. Naturforsch. **40 a,** 968 (1985).
[19] P. A. Mackrodt, J. Fluid Mech. **73,** 153 (1976).
[20] B. Saltzman, J. Atmos. Sci. **19,** 329 (1962).
[21] E. N. Lorenz, J. Atmos. Sci. **20,** 130 (1963).
[22] M. E. Gurtin, The Linear Theory of Elasticity, in: Handbuch der Physik, eds. S. Flügge, C. Truesdell, Springer-Verlag, Berlin 1972.
[23] P. Chadwick and E. A. Trowbridge, Proc. Cam. Phil. Soc. **63,** 1177 (1967).
[24] U. Brosa, Zur Lösung von Randwertproblemen mit Vektorfeldern, Habilitationsschrift, Universität Marburg 1985.